Electronic structure of FeS_2: The crucial role of electron-lattice interaction

V. Eyert*
Hahn-Meitner-Institut, Theory Department, Glienicker Straße 100, D-14109 Berlin, Germany

K.-H. Höck
Institut für Physik, Universität Augsburg, Memminger Straße 6, D-86135 Augsburg, Germany

S. Fiechter and H. Tributsch
Hahn-Meitner-Institut, Department of Solar Energetics, Glienicker Straße 100, D-14109 Berlin, Germany
(Received 29 September 1997)

Using the results of fully self-consistent all-electron first-principles calculations for semiconducting iron pyrite we discuss the major factors governing the semiconducting properties as well as the chemical bonding of this material. The calculations are based on density functional theory within the local density approximation and employ the augmented spherical wave method in its scalar-relativistic implementation. The electronic properties are dominated by strongly hybridized Fe $3d$ and S $3p$ states. The chemical bonding is analyzed using an *ab initio* implementation of the crystal orbital overlap population. Chemical stability is shown to result mainly from the Fe-S bonding. While the upper part of the valence band is formed mainly from Fe $3dt_{2g}$-derived states the conduction band comprises the e_g-derived levels. The conduction band minimum, in contrast, is exclusively due to S $3p$ states, this fact explaining the observed high optical absorption. For the same reason the optical properties are strongly influenced by the short sulfur-sulfur bonds. We demonstrate that only small deviations in the sulfur pair bond lengths involve rather drastic changes of the near-gap electronic states which might even turn the indirect band gap into a direct one. These findings allow us to understand the rather high sensitivity of the optical band gap to the incorporation of defects. Finally, our results open perspectives for photovoltaic applications of FeS_2. [S0163-1829(98)04011-9]

I. INTRODUCTION

The pyrite-type transition metal disulfides MS_2 with M = Fe, Co, Ni, Cu, Zn, Ru have long been attracting scientific and technological interest because of a broad range of electronic, magnetic, and optical properties (see, e.g., Refs. 1–7 just to mention a few). Among these compounds are semiconductors like the van Vleck paramagnet FeS_2 and the wide-band-gap diamagnet ZnS_2. In contrast, CoS_2 is a ferromagnetic metal ($T_C \approx 130$ K) while CuS_2 becomes superconducting.[2,8–10] Much interest has also been focused on the antiferromagnetic insulator NiS_2 which undergoes two magnetic phase transitions at $T_{N_1} \approx 54$ K and $T_{N_2} \approx 31$ K,[2,9–12] and has been interpreted in terms of the Mott-Hubbard-type picture for highly correlated electron systems.[6,10] In general, the changing influence of electron correlations across the series, which is related to the successive filling of the e_g manifold of the crystal-field-split d bands, remains a central issue. A systematic study is favored by the fact that the pyrites from FeS_2 to CuS_2 and the selenides of Co and Ni form solid solutions.[10,13] As a consequence, the occupation of the e_g band can be continuously varied, thus allowing for the construction of comprehensive phase diagrams.[10]

A lot of both experimental and theoretical work has been performed on the pyrite-type transition metal disulfides. Whereas x-ray photoemission spectroscopy (XPS), ultraviolet photoemission spectroscopy (UPS), x-ray absorption spectroscopy (XAS), and bremsstrahlung isochromate spectroscopy (BIS) were used to determine the occupied and unoccupied electronic states[14–21] optical measurements were used to evaluate the band gap.[20,22,23] As a matter of fact, many different numbers for the optical band gap were published ranging from 0.7 eV to 2.62 eV (see, e.g., Refs. 24–26 for an overview). As Ferrer *et al.* and Ennaoui *et al.* pointed out this diversity traces back mainly to differences of samples, experimental techniques, and treatment of the experimental data.[25,26] Most reliable results are obtained from photoconductivity measurements which yield 0.9–0.95 eV and agree with optical and conductivity experiments.[22,26] Raman and IR experiments were guided by the peculiarities of the pyrite structure with its interplay of metal-sulfur and relatively short S-S bonds[27–30] and accompanied by force constant calculations.[31] Susceptibility, magnetization, neutron diffraction, Mössbauer, and perturbed angular correlation (PAC) measurements finally aimed at the low-spin–high-spin question, the formation of local moments, and the resolution of the magnetic structure especially of the Ni member of the series.[8,9,11–13,32–34]

As concerns the theoretical description of the MS_2 compounds qualitative one-electron band schemes and phase diagrams were supplied already by the end of the 1960s.[2,4,35–37] They were complemented by more accurate band calculations mainly on FeS_2 ranging from non-self-consistent tight-binding[38,24] and semiempirical calculations[39] to self-consistent state-of-the-art studies[21,40,41] which, except for the work by Khan, show a remarkably good agreement. However, there are still distinct discrepancies concerning the exact shape of the bands. In particular, the upper valence and

lower conduction bands of FeS_2 and hence the location of the valence band maximum and conduction band minimum are not yet fully resolved. These complications might be traced back to the fact that even the latest calculations involved limiting approximations such as, e.g., an uncomplete basis set[21] or use of the rigid core approximation.[41] In view of the high standard band theory has reached the situation is unsatisfactory and calls for a renewed calculation in order to reactivate materials research on these compounds.

Much interest has focused on iron pyrite FeS_2 for its promising capabilities as a material for photovoltaic applications.[26] This is, of course, related to the high quantum efficiency ($>90\%$) and the high absorption coefficient ($\geqslant 10^5$ cm^{-1} for $h\nu > 1.3$ eV) but also benefits from the nontoxity of the constituents.[42,43] Yet, the rather small value of the optical band gap prohibits optimal use of the solar spectrum. For this reason, many investigations aimed at increasing the band gap, e.g., by alloying with other materials. Recently, we found a considerable increase of the optical band gap by about 0.07 eV on the implantation of only a very small amount ($<5\times10^{20}$ cm^{-3}) of Zn into FeS_2.[44] From the absence of any indications of additional phases and the fact that Zn and Fe are frequently associated in minerals we conclude that the Zn atoms homogeneously substitute for Fe atoms. The aforementioned concentration then corresponds to a Zn content of $\approx 2\%$ and an average Zn-Zn distance of about 15 Å. In view of this small concentration as well as the fact that ZnS_2 is a wide-gap semiconductor with $3d$ states located well below the valence band maximum an explanation of this gap widening exclusively in terms of the electronic states seemed unlikely. Since Zn has a larger atomic radius as compared to iron, we propose instead a mechanism based on crystal structure distortions caused by the incorporation of Zn impurities into iron pyrite and a considerable electron-lattice interaction.[44] The latter would transform the structural deviations into the observed changes of the electronic structure.

In order to get more support for these ideas and to resolve in general the above-mentioned uncertainties of the electronic structure we initiated the present first-principles study. In doing so, we decided to concentrate for the time being on pure FeS_2 and to leave a systematic investigation of the mixed system $Fe_{1-x}Zn_xS_2$ for later work. Hence, we study in a first step the effects of symmetry-conserving deviations from the measured crystal structure without actually taking the Zn impurities into account. In addition, we address the chemical bonding by using the concept of crystal orbital overlap population[45] (COOP) which was recently implemented into the augmented spherical wave (ASW) method.[46]

The paper is organized as follows: Starting out with a short summary of the crystal structure data in Sec. II we outline the method of calculation in Sec. III. Turning to the results we present in Sec. IV A the calculations using the experimentally reported crystal structure whereas in Sec. IV B we look in more detail at the influence of deviations from the ''real'' crystal structure on the electronic structure. Section V finally summarizes the most important results.

II. CRYSTAL STRUCTURE

At room temperature FeS_2 crystallizes in the pyrite structure which is based on a simple cubic (sc) lattice with space group $Pa\bar{3}$ (T_h^6) (Refs. 32, 33, and 43) and lattice constant $a = 5.4160$ Å.[33] We display the crystal structure in Fig. 1. The positions of the atoms and the crystal structure parameter are listed in Table I where the Wyckoff positions ($4a$) and ($8c$) are special cases of the general position (24d): $\pm$(x,y,z), $\pm(\frac{1}{2}-x,-y,\frac{1}{2}+z)$, $\pm(-x,\frac{1}{2}+y,\frac{1}{2}-z)$, $\pm(\frac{1}{2}+x,\frac{1}{2}-y,-z)$ (and cyclic permutations of x,y, and z).

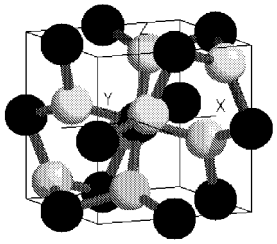

FIG. 1. Crystal structure of FeS_2. Iron and sulfur atoms are printed in black and light gray, respectively.

The pyrite crystal structure is best described in terms of the NaCl structure with the sublattices occupied by iron atoms and the centers of gravity of sulfur atom pairs, respectively. These sulfur dumbbells are oriented along the $\langle 111 \rangle$ axes. Being 2.161 Å their bond length is still shorter than the Fe-S distance of 2.265 Å. Whereas the sulfur atoms are tetrahedrally coordinated by one sulfur and three iron atoms the six nearest-neighbor sulfur atoms at each iron site form slightly distorted octahedra. Due to the deformations of the octahedra, the local symmetry at these sites is reduced from cubic (O_h) to trigonal (C_{3i}). The distorted FeS_6 octahedra are interlinked by common corners and, due to the formation of the $\langle 111 \rangle$ sulfur pairs, have rotated away from the Cartesian axes by about 23°. For a two-dimensional crystal the situation is sketched in Fig. 2. Obviously, the formation of the $\langle 111 \rangle$ sulfur pairs does not destroy the square planar coordination of the iron atoms. Instead, the squares built by the sulfur atoms just shrink and rotate. Since the orientation of the dumbbells conforms with the cubic point group, the underlying Bravais lattice is no longer face centered but simple cubic and the unit cell comprises four formula units. Yet, as we will see below, some features of the electronic structure may still be understood in terms of the face-centered-cubic (fcc) lattice.

According to Bradley and Cracknell the space group $Pa\bar{3}$ (T_h^6) is exceptional among the 230 space groups as it is the only one which is neither an invariant subgroup of any larger space group based on the simple cubic Bravais lattice nor a member of a pair of isomorphic space groups.[47] For this reason, the irreducible wedge of the first Brillouin zone as given in Fig. 3 is twice as big as that of the more familiar

TABLE I. Crystal structure parameters (from Ref. 33).

Atom	Wyckoff positions	Parameter
		x
Fe	($4a$)	
S	($8c$)	0.38484

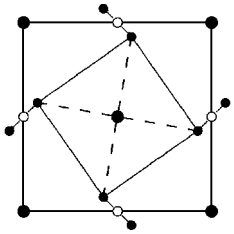

FIG. 2. Two-dimensional analog of the pyrite structure. Big and small solid circles designate iron and sulfur atoms, respectively. Small open circles mark the ideal positions conforming with the rocksalt structure.

monoatomic case and we have to distinguish the high-symmetry points $X=(0,\frac{1}{2},0)$ and $X'=(\frac{1}{2},0,0)$.

III. METHOD OF CALCULATION

Our calculations are based on density functional theory (DFT) and the local density approximation (LDA).[48,49] As a calculational scheme we employ the ASW method[50] in its scalar-relativistic implementation[51,52] (see Refs. 53 and 54 for more recent descriptions). This is the same method as that used in the previous study on FeS_2 by Folkerts *et al.*[21] Since the ASW method uses the atomic sphere approximation (ASA),[55] we had to insert so-called empty spheres into the open crystal structure of FeS_2. These empty spheres are pseudoatoms without a nucleus which are used to model the correct shape of the crystal potential in large voids.[56] In order to minimize the sphere overlap we have recently developed an algorithm[57] which solves the problem of finding optimal empty sphere positions as well as radii of all spheres automatically. As a result, by inserting 32 empty spheres into the simple cubic unit cell of FeS_2 we were able to keep the linear overlap of any two physical spheres below 10% and the overlap of any pair of physical and empty spheres below 18%. The positions of the empty spheres are listed in Table II. In addition to the empty sphere positions the algorithm proposed the following sphere radii: Fe, $2.243a_B$; S, $2.223a_B$; E_1, $1.630a_B$; and E_2, $1.543a_B$.

Our automatically generated result differs considerably from the choice taken by Folkerts *et al.* who, likewise relying on the ASA, faced the same problem of selecting good empty sphere positions and atomic sphere radii.[21] These authors discussed two possible solutions, one using no empty sphere at all and the other with one type of empty sphere. Checking their numbers we found that the first choice leads to a linear overlap of up to 34% whereas with the second choice one can reduce the maximum linear overlap to 30%

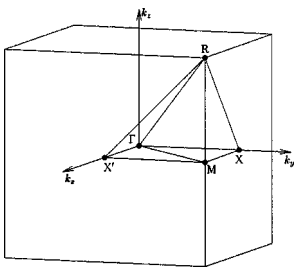

FIG. 3. First Brillouin zone of the simple cubic lattice.

TABLE II. Empty sphere positions.

Atom	Wyckoff positions	Parameters		
		x	y	z
E_1	$(8c)$	0.1935		
E_2	$(24d)$	0.4446	0.1373	0.1980

between physical spheres and 34% between a physical and an empty sphere. Folkerts *et al.* reported on substantial discrepancies of the electronic structure calculated with these two sphere geometries. At the same time, their second choice resulted in a better agreement of the calculated electronic properties with the experimental data from XPS, BIS, and optical experiments.[21] Nevertheless, as we will demonstrate below, there are still substantial improvements of the electronic structure when we use the above listed empty sphere positions and sphere radii from our own algorithm. As a recalculation of the work of Folkerts *et al.* with their second choice of sphere radii, however, revealed, the shortcomings of their band structure result only to a lesser degree from the sphere geometry alone but are rather due to the fact that, with their choice of sphere radii, the selected basis set for the variational procedure was not fully complete.

The basis set used for the present calculations comprises Fe$4s$, $4p$, and $3d$ orbitals, S$3s$, $3p$, and $3d$ orbitals, and $1s$ and $2p$ orbitals of the empty spheres. In addition, $4f$ states of Fe and S as well as empty sphere $3d$ states were included as tails of the aforementioned orbitals (see Refs. 50, 53, and 54 for more details on the ASW method).

The Brillouin zone sampling was done using an increased number of **k** points ranging from 11, 24, and 76 to 176 points within the irreducible wedge. This way we were able to ensure convergence of our results with respect to the fineness of the **k** space grid. Self-consistency was achieved by employing an efficient algorithm for convergence acceleration[58] the convergence criterion for the atomic charges and the total energy being 10^{-8} electrons and 10^{-8} Ry, respectively.

In addition to the calculation of the band structure and the (partial) densities of states we opted for an evaluation of the COOP. The concept of COOP's has been introduced by Hoffmann[45] in order to allow for a discussion of chemical bonding. Roughly speaking the COOP consists of the density of states weighted with nondiagonal elements of the matrix

$$c_i^*(\mathbf{k})S_{ij}c_j(\mathbf{k})=c_i^*(\mathbf{k})\langle\chi_{\mathbf{k}i}(\mathbf{r})|\chi_{\mathbf{k}j}(\mathbf{r})\rangle c_j(\mathbf{k}), \qquad (1)$$

where S_{ij} represents an element of the overlap matrix of the basis functions $\chi_{\mathbf{k}i}(\mathbf{r})$ and the $c_j(\mathbf{k})$ are the coefficients entering the expansion of the wave function in terms of the basis functions. A more detailed description of the COOP's in particular in the context of first-principles DFT calculations has been given in Ref. 59. Positive contributions to the COOP indicate a bonding of the respective orbitals whereas negative terms in Eq. (1) point to antibonding states. The evaluation of the COOP has been recently implemented in the ASW method[46] and already successfully applied to the interpretation of bonding properties of various compounds.[59]

IV. RESULTS AND DISCUSSION

A. Calculations using the experimental crystal structure

To the first approximation, the electronic structure of FeS_2 may be discussed in terms of a molecular orbital pic-

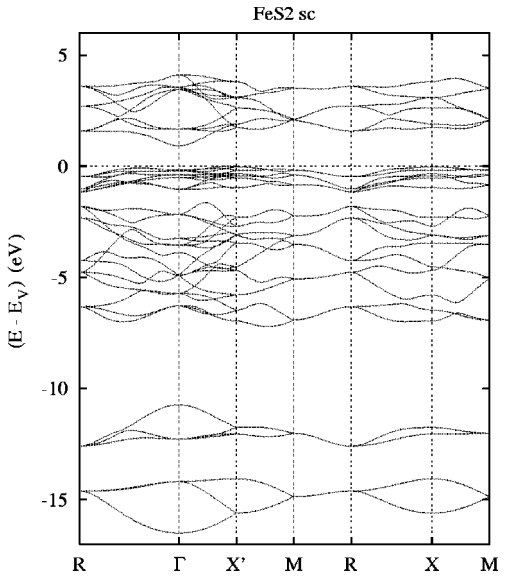

FIG. 4. Electronic bands of FeS_2 along selected symmetry lines within the first Brillouin zone of the simple cubic lattice, Fig. 3. Here and in the following figures energies are given relative to the valence band maximum E_V.

ture where the formation of $(S_2)^{2-}$ pairs leads to five occupied sulfur states per pair. The remaining antibonding $p\sigma^*$ band, in contrast, will be located above the insulating gap. Accordingly, iron turns out to be in a $3d^6$ configuration and has a low-spin $(t_{2g})^6(e_g)^0$ state in octahedral coordination. Since the distortion of the FeS_6 octahedra lowers the symmetry of the crystal field at the iron site from cubic (O_h) to trigonal (C_{3i}), the t_{2g} levels are further split into a low-lying twofold degenerate e_g^π level and a higher a_{1g} singlet.[36,37] For clarity the original e_g level is then designated as the e_g^σ state. Nevertheless, since the deviations from octahedral symmetry are rather small, we still expect that the crystal field splitting is dominated by its cubic part.

To start with the presentation of our own *ab initio* results we show in Fig. 4 the band structure of FeS_2 along selected high-symmetry lines within the first Brillouin zone of the simple cubic lattice, Fig. 3. The corresponding density of states (DOS) is given in Fig. 5 where we have added the dominant partial densities of states.

In Figs. 4 and 5 we clearly identify five groups of bands. In the energy range between 17 and 10 eV below the valence band maximum we observe two groups, each comprising four single bands. Bands are most easily counted along the line M-R where they are fourfold degenerate. According to the partial densities of states these bands almost exclusively trace back to the S $3s$ states which form a bonding and antibonding subset of about 2.5 and 1.8 eV width, respectively. Whereas the large splitting between these two groups of ≈ 3 eV is due to the short S-S distance the intrinsic band widths of both groups mainly result from the dispersion across the fcc lattice formed by the sulfur pairs. This we conclude from the level sequence at the Γ point into a lower nondegenerate and an upper threefold degenerate state, the latter of which results from folding the fcc bands into the simple cubic Brillouin zone (for the antibonding group of bands the sequence of levels is reversed). Further support comes from the striking similarity of the density of states, in particular of the bonding bands to that of a band calculated within the tight-binding approximation for a fcc lattice.[60] These two groups of bands and especially the asymmetric shape of their densities of states compare nicely to the results of the previous band calculations as well as to the XPS core level spectra of van der Heide *et al.*[18] who find the corresponding peaks at -16.4 and -13.3 eV, respectively. The downshift of the experimental peaks by ≈ 1 eV relative to the calculated ones may be explained by the screening of the remaining core hole.

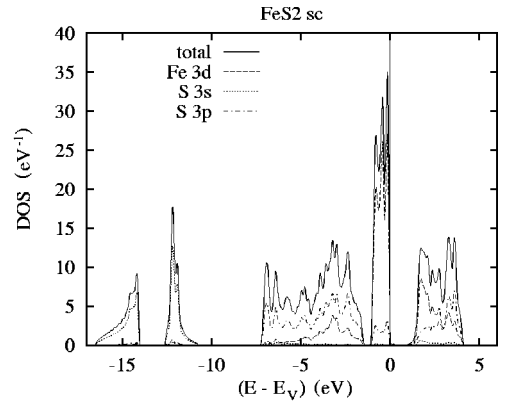

FIG. 5. Total and partial densities of states (DOS) of FeS_2.

In the energy range from -7.3 eV to -1.5 eV we find a group of 20 bands which derive from hybridized Fe $3d$ and S $3p$ orbitals with larger contributions from the latter. Just below the valence band maximum a fourth group of 12 bands appears which mainly originates from iron $3d$ states with a small admixture from sulfur $3p$ states. In the following discussion we will designate these two groups of bands as the lower and upper valence bands, respectively. The conduction band finally comprises likewise 12 bands. They are of Fe $3d$ and S $3p$ character with the relative contributions gradually changing as the energy increases. In particular, the S $3p$ states show up in the pronounced double peak at ≈ 3.5 eV. All other states of Fe and S which are not included in Fig. 5 play only a negligible role in the given energy interval.

The optical band gap separating occupied and unoccupied states amounts to ≈ 0.95 eV. This is in very good agreement with the experimental values ranging from 0.9 to 0.95 eV as deduced from optical and conductivity measurements.[22,26] Nevertheless, we point out that density functional theory, being a ground state theory, is not intended to properly account for the size of the optical band gap (see, e.g., Ref. 59 and references therein). Still, the tendency of the LDA to underestimate the optical band gap is rather sensitive to the driving force for the band separation and has been found to be somewhat reduced in some d band materials where crystal field splitting is of the same order of magnitude and, depending on the nature of the near-gap states, might influence the size of the band gap.[61] This seems to be the case here.

As already mentioned, from the fact that the iron atoms are located at the centers of rotated and slightly distorted FeS_6 octahedra we expect a considerable crystal field splitting of the Fe $3d$ levels into a lower t_{2g} and upper e_g manifold. This is well demonstrated by the partial Fe $3d$ DOS given in Fig. 6 where we have included only one single iron

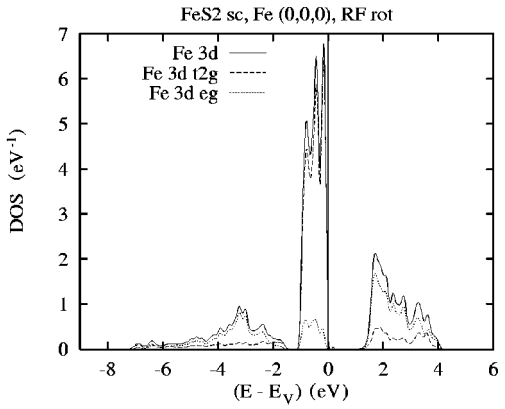

FIG. 6. Partial Fe $3d$ densities of states (DOS) of FeS_2. Note that the selection of orbitals is relative to a rotated reference frame (see text).

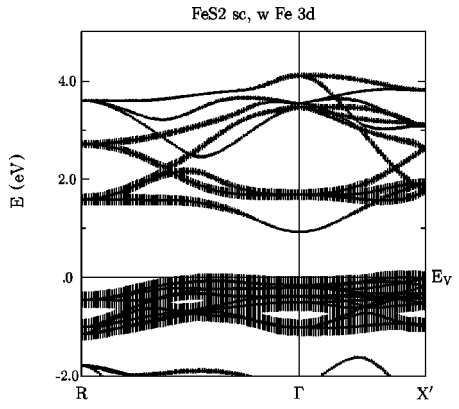

FIG. 8. Electronic bands of FeS_2. The width of the bars given for each band indicates the contribution due to the Fe $3d$ orbitals.

atom. Note that due to the tilting of the FeS_6 octahedra by 23° we had to rotate the frame of reference before performing the projection on the partial $3d$ states. Figure 6 clearly reveals the almost perfect energetical separation of the $3d$ t_{2g} and e_g groups of bands by the crystal field splitting. The former states appear mainly in the upper valence band without any substantial bonding-antibonding splitting. This is different for the e_g levels which, forming σ bonds and hence having a much larger overlap with the sulfur $3p$ orbitals, experience a considerable splitting into bonding and antibonding states with the main peaks at ≈ -3.5 and 2 eV, respectively.

Next we turn to the S $3p$ states. The corresponding partial densities of states of those two sulfur atoms which are near the center of the cubic unit cell are shown in Fig. 7 where we have now rotated the frame of reference such that the local z axis lies parallel to the $\langle 111 \rangle$ line connecting both sulfur atoms. As Fig. 7 clearly reveals, the $3p_x$ and $3p_y$ partial DOS are still identical while the $3p_z$ curve shows distinct deviations. In particular, the latter dominates the unoccupied and hence antibonding S $3p$ states. This becomes rather obvious from the characteristic double peak of the $3p_z$ DOS at about 3.5 eV. The bonding counterpart is found at -6.75 eV whereas the $3p_x$ and $3p_y$ curves dominate in the energy range between ≈ -4 and ≈ -1.5 eV. Hence, among the three sulfur $3p$ bands, the p_z states show the largest bonding-antibonding splitting. This is not suprising since the $3p_z$ states form σ bonds between the two sulfur atoms of a pair whereas the $3p_x$ and $3p_y$ orbitals experience a much smaller overlap via π bonds.

Besides discussing the main peaks of the Fe $3d$ and S $3p$ DOS we focus the reader's attention in particular on the peak of the $3p_z$ DOS at ≈ -3.9 eV as well as on the lowest edge of the conduction band which is exclusively due to the $3p_z$ orbitals without any contributions from the other two $3p$ or the Fe $3de_g$ orbitals. The latter fact is clearly demonstrated in Figs. 8 and 9 where we display the near-gap electronic bands in a special representation. In both figures, each band at each **k** point is given a bar, the length of which is a measure for the contribution from a specified orbital. In particular, we derive the dominating influence of the Fe $3d$ states to the upper valence band from the long bars in Fig. 8. According to Fig. 9 these bands have no bars indicative of S $3p$ states. For the conduction bands we observe strong Fe $3d$ contributions in the energy window from ≈ 1.5 to 3.0 eV, whereas for energies above this range and especially at the lowest edge of the conduction bands S $3p$ dominate. The change of band character from Fe $3d$ to S $3p$ can be clearly observed in the lowest conduction band along the line $R-\Gamma$. As can be seen in Fig. 9, at the Γ point this band is exclusively due to S $3p$ states but, due to hybridization with

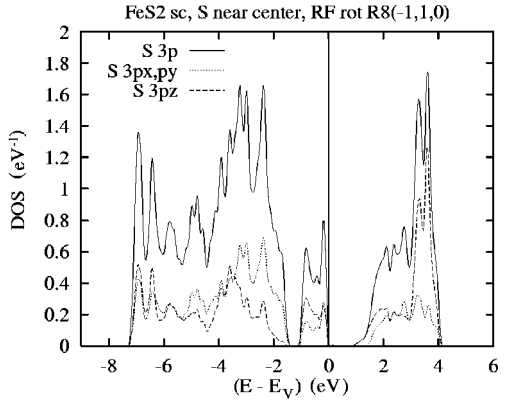

FIG. 7. Partial S $3p$ densities of states (DOS) of FeS_2. Note that the selection of orbitals is relative to a rotated reference frame (see text).

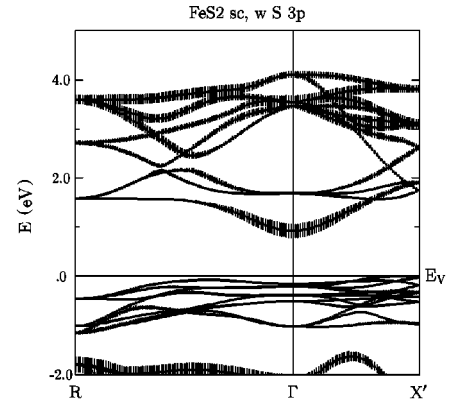

FIG. 9. Electronic bands of FeS_2. The width of the bars given for each band indicates the contribution due to the S $3p$ orbitals.

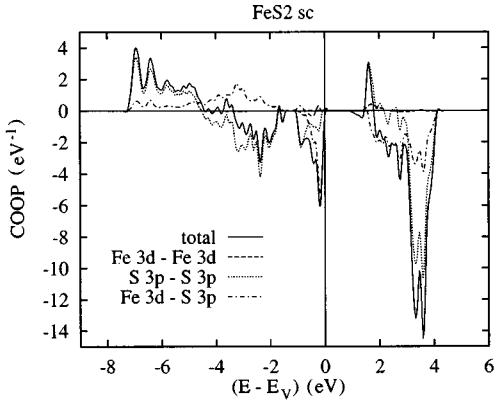

FIG. 10. Total and partial crystal orbital overlap populations (COOP) of FeS_2.

the Fe $3d$ states, loses this dominance as one goes to the R point. In contrast, in the middle between both points the band at 2.5 eV takes over the S $3p$ character and keeps it until the R point is reached at about 3.7 eV. From a different point of view we interprete the band starting at Γ at ≈ 1.0 eV and dispersing almost linearly to 3.7 eV at the R point as the S $3p$ band which hybridizes with the dispersionless e_g bands in the energy region between 1.5 and 2.5 eV half way between Γ and R. The situation is thus not unlike that in elementary Cu where the lowest s-like state hybridizes with the $3d$ states just below the Fermi energy but again assumes the original $4s$ character above E_F.[59]

As for the S $3s$ bands the states at -3.9 eV and at the conduction band minimum originate from a dispersion of the sulfur $3p$ bands accross the underlying fcc lattice. Hence, the formation of the sulfur-dominated bands evolves mainly in two steps. First, due to the close coupling of the sulfur pairs, the S $3p$ states are strongly split into bonding and antibonding states which, in case of the $3p_z$ orbitals, leads to the rather sharp double peaks at -6.75 and 3.5 eV. Once these effective sulfur pair states have been formed they disperse across the fcc lattice but are folded back to the smaller Brillouin zone of the simple cubic lattice. As a consequence, both the bonding and antibonding subband have a considerable bandwidth. Finally, we arrive at the rather surprising conclusion that the optical band gap separates Fe $3d$ t_{2g} and S $3p_z$ orbitals and hence, although being strongly influenced by the crystal field splitting, cannot be described exclusively in terms of it. In contrast, the different orbital composition of the valence band maximum and the conduction band minimum provides a natural explanation of the high optical absorption.

We complement the previous discussion by addressing the chemical bonding of FeS_2 via the crystal orbital overlap population as shown in Fig. 10. The COOP curves display the rather ''canonical'' behavior being positive (bonding) and negative (antibonding) in the low- and high-energy regions of a band. In case of the sulfur-sulfur overlap this is nicely visible for both the valence and the conduction bands separately, the absolute values being higher in the latter. Below -4.5 eV we find bonding S-S σ and π bands. The corresponding antibonding states, in contrast, are separated in energy. S-S π^* states lead to the negative COOP in the interval from -4.5 to -1.5 eV whereas S-S σ^* states dominate in the upper half of the conduction band. Sulfur states in the upper valence band and the lower half of the conduction band finally are rather nonbonding. As a consequence of the complete filling of the sulfur π and π^* bonds the net contribution of the occupied sulfur-sulfur bonds to the chemical stability is rather small. The same holds for the metal-metal bonding, the effect of which is almost negligible due to the large Fe-Fe separation. The dominating contribution to the chemical stability results from the overlap of Fe $3d$ and S $3p$ orbitals. They lead to a COOP curve which is positive throughout the lower valence band and negative only in the t_{2g}-derived band and in the conduction band. Bonding Fe $3d$–S $3p$ contributions result from σ bonds of the e_g and S $3p$ states as well as π bonds formed by overlap of the t_{2g} and the $3p$ states. The corresponding antibonding π^* and σ^* orbitals, in contrast, show up in the upper valence band and the lower half of the conduction band, respectively. Since a large portion of these antibonding states is shifted to the bands above the insulating gap, the iron-sulfur bonding can be identified as the decisive factor for the stability of FeS_2.

There is an overall good agreement of the calculated electronic structure with experimental data. This holds especially for the photoemission measurements which find the upper valence band of 0.8–1.3 eV width at 0.8–0.9 eV below the valence band maximum[15,16,18,21] whereas the calculation locates this band at about -0.6 eV. According to Li *et al.* the S $3p$ dominated bands extend from -8.6 to -1.8 eV.[15] XPS spectra by Ohsawa *et al.* clearly reveal a main peak at -4 eV and a pronounced shoulder at about -7 eV.[16] From our calculation we get the S $3p$ contribution in the interval from -7.3 to -1.5 eV with dominant peaks at about -3.2 eV and -7 eV. Again attributing the relative shift of the lower edge to screening effects we observe almost quantitative agreement. From $K\beta$ emission and K absorption spectra Sugiura *et al.* extract values of 2.7 and 5.9 eV for the position of the upper valence and conduction bands, respectively relative to the main peak of the occupied S $3p$ bands[17,19] which compare very good with the calculated numbers of 2.6 and ≈ 6.5 eV, respectively. Finally, the calculated positions of the unoccupied S $3p$ states conform very well with the value of 3.3 eV as derived from BIS measurements by Folkerts *et al.*[21] Still, it would be interesting to compare our results to angle-resolved photoemission data which, however, do not seem to be published so far. In passing we mention that our results confirm the magnetic measurements by giving a low-spin state for the Fe $3d$ orbitals.[8]

Comparing our results to the previous band calculations we likewise arrive at satisfactory agreement as concerns the band positions and edges. This is true in particular for the calculations by Bullett,[24] by Folkerts *et al.*,[21] and by Temmerman *et al.*,[40] their densities of states being almost identical to ours. Visible deviations shows the calculation of Zhao *et al.* which place the S $3s$-derived and occupied $3p$-derived bands considerably lower,[41] this fact being in conflict with the values given by Sugiura *et al.* for the relative band positions.[17]

Although all electronic structure calculations including our own agree in finding an indirect band gap, there exist some deviations concerning the extremal band positions. Ob-

viously, they trace back to the differences showing up for the near-gap electronic states which we already mentioned in the Introduction. Concentrating on only the latest state-of-the-art work we witness, however, some agreement coming up. Folkerts *et al.* reported on a valence band maximum (VBM) lying not on a high-symmetry line but somewhere within the first Brillouin zone and found the conduction band minimum (CBM) at $\approx 0.7(\frac{1}{2},\frac{1}{2},\frac{1}{2})$ (in units of $2\pi/a$).[21] From their band structure it seems likely that the VBM is located near the X point. The latter fact would compare well with the findings of Zhao *et al.* who locate the VBM at the X point and the CBM at the center of the first Brillouin zone.[41] With respect to the VBM we conclude from the band structure as well as from a scan through the first Brillouin zone on a mesh of $30\times30\times30$ points that the valence band maximum is located at the point (0.0,0.0,0.4136), which indeed is in the vicinity of the X point and thus compares well with the result of Zhao *et al.*[41]

At a first glance, agreement for the CBM seems to be less satisfactory. Yet, besides clearly locating the CBM at the Γ point and thus confirming the results of Zhao *et al.*, we were able to assign the deviating result of Folkerts *et al.* to their use of an incomplete basis set. This was clearly revealed by a recalculation of their work. To be specific, with the sphere geometry and basis set reported by these authors we get an occupation of the Fe $4f$ states of 0.45 electrons which is not accounted for by an inclusion of these states into the secular matrix (see, e.g., Refs. 50, 53, and 54 for details on the ASW and related methods). We are thus able to note agreement of the remaining band studies and to summarize the results to the effect that the VBM and CBM reside near the X point at (0.0,0.0,0.4136) and at the Γ point, respectively.

B. Role of pressure and crystalline distortions

Still, we did not yet pay much attention to the factors which might influence the optical band gap. Indeed, it would be desirable to identify mechanisms which change the size or the indirect nature of the gap or modify the composition of the near-gap states. More insight into such mechanisms would finally allow us to address the question of why incorporation of small amounts of Zn into FeS_2 leads to the experimentally observed widening of the optical band gap.[44]

Since it is unlikely that the changes of the electronic structure of FeS_2 on the substitution of Zn for Fe can be explained from the differences in the electronic configurations alone, we propose a rather strong influence of the accompanying distortions of the crystal structure due to the larger atomic radius of Zn in addition to a considerable electron-lattice interaction. Nevertheless, we decided to stay for the time being with pure FeS_2 and to study from a more general point of view the sensitivity of the electronic structure to symmetry-conserving deviations from the measured crystal structure. Obviously, such an investigation not only serves as a necessary prerequisite to a solution of the forementioned problem but is an interesting topic in itself.

To start with, we simulated in a first step the application of external pressure and performed a fully self-consistent calculation for FeS_2 with the lattice constant reduced by 5%. As a result, there are mainly two effects. As expected, hydrostatic pressure leads to a broadening of all bands without noticeable reorderings of the electronic states. At the same time, there is a corresponding reduction of the total and partial DOS. Second, the main peaks of the lower valence and the conduction band experience rather large shifts to lower and higher energies, respectively. For the lowest and highest peaks the shifts are even as large as about 1 eV. In particular, the pronounced S $3p_z$-dominated double peaks at about -6.75 and 3.5 eV move to ≈ -7.5 and ≈ 4.4 eV, respectively. To a lesser degree the same happens to the peaks between -4 and -2 eV as well as at 2 eV. These large shifts of all electronic states away from the valence band maximum add to the effect of the aforementioned band broadening and, as a consequence, the size of the optical band gap remains essentially unchanged.

This result conforms quite well with pressure experiments mentioned by Schlegel and Wachter.[22] These authors report on a hydrostatic pressure study by Batlogg who finds a slight blueshift of 2×10^{-6} eV bar^{-1} of the optical absorption edge. According to Schlegel and Wachter this can be explained by the increased crystal field splitting between the iron $3d$ t_{2g} and e_g levels on the application of pressure.[22] Although fully correct, in view of the information gained in the previous subsection this interpretation appears to be incomplete. In particular, it cannot explain the largest shifts appearing for the S $3p_z$ bands which, however, were not accessible by the measurements of Schlegel and Wachter.

Guided by the discussion of Sec. IV A we describe the gross features of the electronic structure in terms of three different energies, namely, the crystal field splitting, Δ_{CEF}, the bonding-antibonding splitting due to the overlap of Fe $3d$ e_g and S $3p$ orbitals, Δ_{e_gp}, and, finally, the strong bonding-antibonding splitting due to the S-S $3p_z$ overlap, Δ_{p_z}. In this rather crude scheme we have not included splittings due to the $3d$ t_{2g}-$3p$ π-type overlap as well as the π bonds within the sulfur pairs both of which are much smaller than the previous three energies. On the application of isotropic pressure, all three of the aforementioned energies are likewise increased, this resulting in an overall spreading of the band structure. As a consequence, we witness not only a band broadening but at the same time the bands shift apart to a similar degree. Since the crossover from bonding to antibonding states as well as the separation of the $3d$ t_{2g} and the main part of the e_g states appears near or at the valence band maximum, the optical band gap finally is not affected.

The situation becomes more complicated in the second part of our simulation. Here we concentrate on the variation of the internal x parameter which determines the sulfur position. To be specific, we again performed fully self-consistent calculations for FeS_2 but now changed the internal sulfur parameter to $x=0.380\,84$ and $x=0.388\,84$, respectively which are just below and above the experimental value of $x=0.384\,84$ listed in Table I. The resulting band structures are shown in Figs. 11 and 12.

Again, the results are rather surprising. First of all, we observe a large shift of the optical band gap of about 0.67 eV when going from $x=0.380\,84$ to $x=0.388\,84$, hence moving the sulfur atoms by less than 1% of the lattice constant. Obviously, this change of the band gap is due to the equivalent shift of the conduction band minimum relative to the centers of gravity of both the valence and conduction bands which

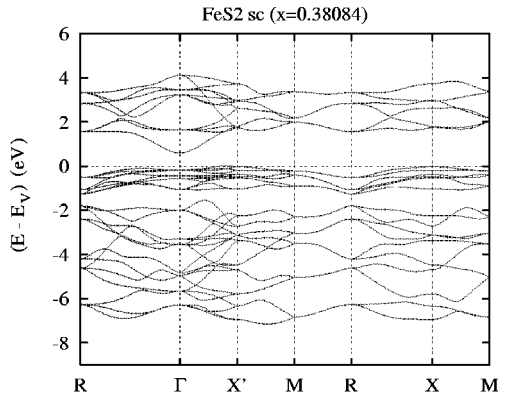

FIG. 11. Electronic bands of distorted FeS_2.

stay essentially inert. From the large shift of the CBM we might even expect that for larger values of the x parameter FeS_2 turns over to a direct gap semiconductor which, of course, would have great implications for the optical properties. Indeed, this trend was confirmed by an additional calculation for $x=0.390\,84$. A shift of similar size as that of the CBM is observed only for the single band which in Fig. 4 can be found at -3.9 eV at the Γ point and moves to -3.6 and -4.3 eV in Figs. 11 and 12. Furthermore, there is a noticeable shift of the sulfur $3p_z$-dominated double peak at about 3.5 eV which moves by approximately 0.5 eV. As a consequence, the total width of the conduction band is reduced.

We thus conclude that variation of the x parameter affects almost entirely the S $3p$ states, especially the $3p_z$ states. Their response to the changes of the crystal structure is essentially twofold. First, increase of the sulfur x parameter leads to a closer coupling of the sulfur pairs and hence to a larger bonding-antibonding splitting. This is revealed by the shifts of the $3p_z$ double peaks. Second, the increase of the x parameter, while shortening the sulfur-sulfur bonds, at the same time reduces the hopping across the lattice. For this reason the dispersion of the $3p_z$ bonding and antibonding bands decreases this leading to the observed downshift of the $3p_z$ state at -3.9 eV at the Γ point as well as to the corresponding upshift of the CBM. From these results we conclude that the sulfur sublattice of FeS_2 should be rather discussed in terms of a molecular S_2 crystal. Furthermore, we identify the reduced dispersion across the lattice as the main mechanism responsible for the rise of the CBM and the accompanying widening of the optical band gap. This effect is supported by the shift of the antibonding double peak at 3.5 eV which pulls the CBM even further to higher energies.

Of course, the latter effect cannot be obtained by the application of pressure which, while likewise increasing the bonding-antibonding splitting, supports hopping between the S_2 molecules by reducing the lattice constant and thus leads to an increase of the $3p_z$ band width. As a result, the CBM would move down (relative to the antibonding double peak) which is indeed observed.

Still, we may ask why the Fe $3d$-dominated bands and, in particular, the crystal field splitting Δ_{CEF} as well as the bonding-antibonding splitting due to the overlap of Fe $3de_g$ and S $3p$ orbitals, Δ_{e_gp}, are almost unaffected by the changes of the sulfur x parameter. From the increase of x we would rather expect a reduced crystal field splitting and hence a lowering of the e_g states in the lower part of the conduction band. At the same time, the e_g-p overlap, i.e., Δ_{e_gp}, should decrease and again the lower half of the conduction band should move downwards. However, we observe neither of these two effects. This may be explained in a rather simple manner from the projection of the pyrite structure, Fig. 2. Obviously, any change of the x parameter affects first of all the length of the sulfur-sulfur bond. Its implications for the geometry of the FeS_6 octahedron, in contrast, are much smaller since the movement of the sulfur atoms relative to the central iron atoms has a substantial tangential component which leads to a much reduced effect on the size of the octahedron and, even more important, preserves the square planar coordination.

We thus arrive at the conclusion that the crystal field splitting plays only a minor role for the optical properties of FeS_2. In contrast, it is rather the bond length of the S_2 molecules which turns out to be the key parameter to a dedicated and strong influence on the S $3p$ states, in particular, $3p_z$ states, this fact revealing a substantial electron-lattice interaction. The latter in turn tunes the energetical position of the conduction band minimum and thereby the optical band gap.

In this context it is interesting to recall the results of Raman measurements which demonstrated that the sulfur-sulfur bond in FeS_2 is rather soft as compared to that of other pyrite type transition metal chalcogenides.[30] As a consequence, one expects that on the application of external isotropic pressure the interatomic distances are reduced to a different degree and, in particular, that the sulfur-sulfur bond compression is larger than that of the Fe-S bonds. Hence, the resulting band structure should include both the effects of scaling of the lattice constant and increase of x: On the application of pressure we would expect the band structure to resemble that of Fig. 12 with an additional broadening of all bands. This finally yields a conclusive understanding of the blueshift of the optical band gap as observed by Batlogg, cited in Ref. 22.

We are finally able to sketch a possible scenario for the substitution of Zn atoms for Fe. From the larger atomic radius of Zn as compared to Fe we can easily imagine that each Zn impurity will push apart its six nearest-neighbor sulfur atoms. This might have two different consequences for the corresponding S_2 molecules. They will be either rigidly

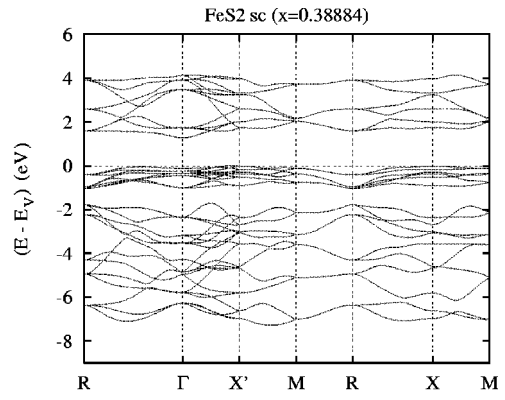

FIG. 12. Electronic bands of distorted FeS_2.

pushed away or else compressed with the distances to the neighboring Fe atoms being essentially unchanged. Of course, any combination of both effects might be also possible. From the previous discussion, however, we expect the second alternative to be the more likely one. In case the sulfur pairs are compressed we expect the CBM to rise because of the mechanisms outlined before. If, however, the bond length of the S_2 molecules were preserved, they would shift away from the ideal positions of the rocksalt structure, this leading to a structural disorder. Again, the dispersion of S $3p_z$ states across the lattice were affected and we would obtain an upshift of the CBM. Hence, in both cases introduction of Zn impurities will push the CBM to higher energies and, most important, while addressing the band dispersion of the $3p_z$ orbitals across the lattice, in both cases the effect is of rather long range. Hence we expect it to show up already for a small amount of Zn impurities which indeed is observed in experiment.

V. CONCLUSION

In the present work first-principles ASW calculations were used to describe the electronic properties of iron pyrite. Chemical stability as investigated by the COOP results from overlap of crystal-field-split Fe $3d$ t_{2g} and e_g orbitals with the sulfur ligand $3p$ states. Hybridization of the latter with the e_g orbitals leads to lower valence and conduction bands whereas the relatively narrow upper valence band stems mainly from t_{2g} states.

Formation of strong σ bonds within the sulfur pairs leads to large bonding-antibonding splitting of the S $3p_z$ states. Dispersion of these states across the lattice causes a considerable bandwidth and places the antibonding states at the conduction band minimum which is thus rather sensitive to the σ bonds. The difference in band characters at the valence band maximum and the conduction band minimum, finally, gives a natural explanation of the high optical absorption.

The influence of the electron-lattice interaction has been probed by simulating both external pressure and changes of the sulfur-sulfur distance. The former leads to the expected band broadening which is accompanied by a spread of all band centers due to an increased crystal field as well as bonding-antibonding splittings and hence does not change the optical band gap. A change of the sulfur x parameter, in contrast, causes drastic changes which can be partially traced back to an increase of the bonding-antibonding splitting of the S $3p_z$ bands on shortening the S_2 bond length. The main effect, however, originates from a disturbance of the dispersion across the lattice, resulting in a reduced bandwidth of the $3p_z$ antibonding band and an upshift of the conduction band minimim. Being a long-range effect it is sensitive to only small disturbances of the crystal structure.

Hence, FeS_2, despite being a transition metal chalcogenide with an unfilled d shell, is extraordinary insofar as its electronic structure as well as its response to crystal structure distortions is almost entirely determined by the sulfur ligand $3p$ states.

ACKNOWLEDGMENTS

We are indebted to M. Birkholz, HMI Berlin, for fruitful discussions and a critical reading of the manuscript.

*Electronic address: eyert@physik.uni-augsburg.de

[1] R. A. Munson, W. DeSorbo, and J. S. Kouvel, J. Chem. Phys. **47**, 1769 (1967).
[2] T. A. Bither, R. J. Bouchard, W. H. Cloud, P. C. Donohue, and W. J. Siemons, Inorg. Chem. **7**, 2208 (1968).
[3] H. S. Jarrett, W. H. Cloud, R. J. Bouchard, S. R. Butler, C. G. Frederick, and J. L. Gillson, Phys. Rev. Lett. **21**, 617 (1968).
[4] J. A. Wilson and A. D. Yoffe, Adv. Phys. **18**, 193 (1969).
[5] J. A. Wilson and G. D. Pitt, Philos. Mag. **23**, 1297 (1971).
[6] S. Ogawa, S. Waki, and T. Teranishi, Int. J. Magn. **5**, 349 (1974).
[7] K. Kikuchi, T. Miyadai, H. Itoh, and T. Fukui, J. Phys. Soc. Jpn. **45**, 444 (1978).
[8] S. Miyahara and T. Teranishi, J. Appl. Phys. **39**, 896 (1968).
[9] K. Adachi, K. Sato, K. Yamanchi, and M. Ohashi, J. Phys. Soc. Jpn. **32**, 573 (1972).
[10] S. Ogawa, J. Appl. Phys. **50**, 2308 (1979).
[11] J. M. Hastings and L. M. Corliss, IBM J. Res. Dev. **14**, 227 (1970).
[12] T. Miyadai, K. Kikuchi, and Y. Ito, Physica B & C **86-88B**, 901 (1977).
[13] X. Yao, Y.-K. Kuo, D. K. Powell, J. W. Brill, J. M. Honig, Phys. Rev. B **56**, 7129 (1997).
[14] G. Wiech and E. Zöpf, J. Phys. (Paris) Colloq. **32**, C4-200 (1971).
[15] E. K. Li, K. H. Johnson, D. E. Eastman, and J. L. Freeouf, Phys. Rev. Lett. **32**, 470 (1974).
[16] A. Ohsawa, H. Yamamoto, and H. Watanabe, J. Phys. Soc. Jpn. **37**, 568 (1974).
[17] C. Sugiura, I. Suzuki, J. Kashiwakura, and Y. Gohshi, J. Phys. Soc. Jpn. **40**, 1720 (1976).
[18] H. van der Heide, R. Hemmel, C. F. van Bruggen, and C. Haas, J. Solid State Chem. **33**, 17 (1980).
[19] C. Sugiura, J. Chem. Phys. **74**, 215 (1981).
[20] S. Suga, M. Taniguchi, S. Shin, M. Seki, S. Shibuya, K. Sato, and T. Yamaguchi, Physica B & C **117B&118B**, 353 (1983).
[21] W. Folkerts, G. A. Sawatzky, C. Haas, R. A. de Groot, and F. U. Hillebrecht, J. Phys. C **20**, 4135 (1987).
[22] A. Schlegel and P. Wachter, J. Phys. C **9**, 3363 (1976).
[23] W. W. Kou and M. S. Seehra, Phys. Rev. B **18**, 7062 (1978).
[24] D. W. Bullett, J. Phys. C **15**, 6163 (1982).
[25] I. J. Ferrer, D. M. Nevskaia, C. de las Heras, and C. Sánchez, Solid State Commun. **74**, 913 (1990).
[26] A. Ennaoui, S. Fiechter, Ch. Pettenkofer, N. Alonso-Vante, K. Büker, M. Bronold, Ch. Höpfner, and H. Tributsch, Sol. Energy Mater. Sol. Cells **29**, 289 (1993).
[27] H.-D. Lutz, G. Kliche, and H. Haeuseler, Z. Naturforsch. A **36**, 184 (1981).
[28] H. Vogt, T. Chattopadhyay, and H. J. Stolz, J. Phys. Chem. Solids **44**, 869 (1983).
[29] H.-D. Lutz, G. Schneider, and G. Kliche, J. Phys. Chem. Solids **46**, 437 (1985).
[30] C. Sourisseau, R. Cavagnat, and M. Fouassier, J. Phys. Chem. Solids **52**, 537 (1991).
[31] H.-D. Lutz, P. Willich, and H. Haeuseler, Z. Naturforsch. A **31**, 847 (1976).
[32] S. L. Finklea III, L. Cathey, and E. L. Amma, Acta Crystallogr., Sect. A: Cryst. Phys., Diffr., Theor. Gen. Crystallogr. **32**, 529 (1976).

[33] E. D. Stevens, M. L. DeLucia, and P. Coppens, Inorg. Chem. **19**, 813 (1980).
[34] W. Müller, H. H. Bertschat, K. Biedermann, R. Kowallik, E. Lahmer-Naim, H.-E. Mahnke, S. Seeger, W.-D. Zeitz, S. Fiechter, and H. Tributsch, Phys. Rev. B **41**, 8624 (1990).
[35] J. A. Wilson, Adv. Phys. **21**, 143 (1972).
[36] J. B. Goodenough, J. Solid State Chem. **3**, 26 (1971).
[37] J. B. Goodenough, J. Solid State Chem. **5**, 144 (1972).
[38] M. A. Khan, J. Phys. C **9**, 81 (1976).
[39] S. Lauer, A. X. Trautwein, and F. E. Harris, Phys. Rev. B **29**, 6774 (1984).
[40] W. M. Temmerman, P. J. Durham, and D. J. Vaughan, Phys. Chem. Miner. **20**, 248 (1993).
[41] G. L. Zhao, J. Callaway, and M. Hayashibara, Phys. Rev. B **48**, 15 781 (1993).
[42] A. Ennaoui, S. Fiechter, W. Jaegermann, and H. Tributsch, J. Electrochem. Soc. **133**, 97 (1986).
[43] M. Birkholz, S. Fiechter, A. Hartmann, and H. Tributsch, Phys. Rev. B **43**, 11 926 (1991).
[44] K. Büker, S. Fiechter, V. Eyert, and H. Tributsch (unpublished).
[45] R. Hoffmann, *Solids and Surfaces: A Chemist's View of Bonding in Extended Structures* (VCH, New York, 1988).
[46] V. Eyert and S. F. Matar (unpublished).
[47] C. J. Bradley and A. P. Cracknell, *The Mathematical Theory of Symmetry in Solids* (Clarendon Press, Oxford, 1972).
[48] P. Hohenberg and W. Kohn, Phys. Rev. **136**, B864 (1964).
[49] W. Kohn and L. J. Sham, Phys. Rev. **140**, A1133 (1965).
[50] A. R. Williams, J. Kübler, and C. D. Gelatt, Jr., Phys. Rev. B **19**, 6094 (1979).
[51] D. D. Koelling and B. N. Harmon, J. Phys. C **10**, 3107 (1977).
[52] H. Gollisch and L. Fritsche, Phys. Status Solidi B **86**, 145 (1978).
[53] J. Kübler and V. Eyert, in *Electronic and Magnetic Properties of Metals and Ceramics*, edited by K. H. J. Buschow (VCH Verlagsgesellschaft, Weinheim, 1992), pp. 1–145.
[54] V. Eyert, Ph.D. thesis, Technische Hochschule Darmstadt, 1991.
[55] O. K.Andersen;, Phys. Rev. B **12**, 3060 (1975).
[56] O. K. Andersen, A. P. Postnikov, and S. Yu. Savrasov, in *Applications of Multiple Scattering Theory to Materials Science*, edited by W. H. Butler, P. H. Dederichs, A. Gonis, and R. L. Weaver, MRS Symposia Proceedings No. 253 (Materials Research Society, Pittsburgh, 1992), p. 37.
[57] V. Eyert (unpublished).
[58] V. Eyert, J. Comput. Phys. **124**, 271 (1996).
[59] V. Eyert, in *Density Functional Methods: Applications in Chemistry and Materials Science*, edited by M. Springborg (Wiley, Chichester, 1997), pp. 233–304.
[60] R. J. Jelitto, J. Phys. Chem. **30**, 609 (1969).
[61] L. F. Mattheiss, J. Phys. Condens. Matter **8**, 5987 (1996).